

Crude extract of Wintersweet (*Chimonanthus praecox*) as Corrosion Inhibitor for Mild Steel in Hydrochloric Acid

Kun Cao*, Leilie Yu, Lan Wang, Xian He

Department of Chemistry & Chemical Engineering, Neijiang Normal University, Neijiang, Sichuan, 641112, PR China

*E-mail: kevin_cao0811@126.com.

Received: 2 December 2020 / Accepted: 20 February 2021 / Published: 31 March 2021

Anticorrosion properties of the wintersweet leaf crude extract (WSLCE) were tested in relationship to the mild steel corrosion in 1 M HCl using gravimetric analysis as well as potentiodynamic polarization and electrochemical impedance tests. The anticorrosive efficiency of WSLCE increased from 76.4% to 91.5% as its content in the solution was increased from 0.1 to 1.0 g/L, respectively. WSLCE behaved as a mixed-type cathodic inhibitor. Extensive characterization of the corrosion products (by SEM, AFM, FTIR, and XPS) showed that WSLCE was adsorbed by the steel surface. Thin WSLCE layer formed on the mild steel surface prevented electron exchange between the steel and HCl, impeding corrosion.

Keywords: anticorrosion; leaf crude extract; inhibitor; adsorption; electrochemical methods

1. INTRODUCTION

Metal corrosion, caused by the electrochemical and chemical reactions between metals and their surroundings, compromises the structural integrity of the metal [1]. Often, corrosion cannot be stopped, but it can be slowed down and mitigated. Some anti-corrosion methods include the usage of corrosion inhibitors [2]. Various N-, S-, and O-, as well as π -electron-containing organic compounds, are very promising as anticorrosion inhibitors [3-8]. Several synthetic organic materials demonstrated very effective corrosion inhibition properties; however, some of them cannot be widely used due to their harmfulness to humans and the environment [9]. Therefore, the development of non-toxic and environmentally friendly corrosion inhibitors, which are also inexpensive and can be prepared on a large scale, recently gained popularity [10-12]. Several of such inhibitors are based on plant extracts [13-15],

Especially those containing active ingredients capable of inhibiting metal corrosion [16-18]. For example, 2-hydroxy-1,4-naphthoquinone extracted from henna leaves showed 95% inhibition efficiency

when used to protect carbon steel [14]. The high inhibition efficiency of 96% was also reported for polyphenol, which is the main constituent of pomegranate peel crude extract [19].

Chimonanthus praecox Link (also called wintersweet) is a medium-sized deciduous shrub, endemic to China. It is widely grown in small and medium-size gardens and pots and used as a cut-flower and in traditional Chinese remedies against cough and rheumatic arthritis [20]. Wintersweet contains flavonoids and coumarins, including kaempferol (KF), rutin (RT), scopoletin (SPT), and scopolin (SP) [21]. However, the usage of wintersweet leaf crude extract (WSLCE) as a corrosion inhibitor in the HCl environment was not reported in the literature. Therefore, in this work, we studied the inhibition efficiency of WSLCE in relationship to mild steel corrosion. First, WSLCE was analyzed by Fourier transform infrared (FTIR) spectroscopy. WSLCE anti-corrosion performance at different temperatures was analyzed electrochemically and gravimetrically. The interactions between WSLCE and steel surface were assessed using FTIR and X-ray photoelectron spectroscopy (XPS) data. The scanning electron and atomic force microscopies (SEM and AFM, respectively) were applied for steel surface characterization. A possible mechanism of steel inhibition by WSLCE was proposed based on data obtained from Langmuir adsorption isotherm and zero charge potential.

2. EXPERIMENTS

2.1. Materials and instruments

The Fresh wintersweet leaves were collected from the campus of Neijiang Normal University. Hydrochloride acid and anhydrous ethanol were purchased from Aladdin Chemistry Company, and used as received without further treatment. Mild steel specimens composition (wt. %) was: 99.07% Fe, 0.55% Mn, 0.19% Si, 0.14% C, 0.03% P and 0.02% S, and were purchased from the Shengxin Technology Co., Ltd.

2.2 Preparation of WSLCE and corrosion solutions

Fresh wintersweet leaves were washed with distilled water, dried overnight at 333 K, and then ground to powder. 50 g of this powder was then soaked in 1.0 L of distilled water (heated to 60 °C) for 60 min. The resulting brown liquid was then concentrated with a rotary evaporator. For FTIR measurements, the powder was additionally dried for 24 h at 60 °C in a vacuum.

1 M HCl, used as a corrosion medium, was prepared by diluting concentrated HCl. Mild steel (type Q235) served as a working electrode. All steel samples were treated with SiC paper (with 400 and 1000 grit sizes) and then by alumina polishing powder with 0.3 μm average particle size. After polishing, the samples were washed with distilled water, ethanol and acetone, and then dried at room temperature.

2.3 Gravimetric analysis

Gravimetric experiments were performed according to the ASTM G1-03 using corrosive media containing different WSLCE concentrations. Experiments were performed at 298, 308, and 318 K.

The average weight losses of the mild steel samples were then used to calculate the corrosion rate (Equation 1) and inhibition efficiency (Equation 2), as shown below:

$$CR(\text{mm per year}) = \frac{87600 \times \Delta w(\text{g})}{d(\text{g} \cdot \text{cm}^{-3}) \times A(\text{cm}^2) \times t(\text{h})} \quad (1),$$

$$\eta(\%) = \frac{CR - CR_{inh}}{CR} \times 100 \quad (2),$$

where Δw is the weight loss, d is the steel density (equal to $7.85 \text{ g} \cdot \text{cm}^{-3}$), A is the sample surface area (equal to 23 cm^2), and t is the immersion time (equal to 3 h).

2.4 Electrochemical characterization

The electrochemical tests were performed using an Ivium 3-electrode workstation with a 1 cm^2 steel piece acting as a working electrode, Pt acting as a counter electrode as well as Ag|AgCl junction acting as a reference electrode. Prior to the tests, all electrodes were soaked in the test solution for 0.5 h to stabilize the system.

Electrochemical impedance spectroscopy (EIS) was performed using a potentiostatic mode at the OCP at 10 mV amplitude in the 100 kHz-10 mHz range. Polarization curves were recorded at $1 \text{ mV} \cdot \text{s}^{-1}$ scan rate in the -700~-200 mV range (vs. reference electrode). The resulting data were then used to calculate WSLCE efficiency by Eq. 3 and Eq. 4:

$$\eta_R(\%) = \frac{R_{ct} - R_{ct}^0}{R_{ct}} \times 100 \quad (3),$$

$$\eta_i(\%) = \frac{i_{corr}^0 - i_{corr}}{i_{corr}^0} \times 100 \quad (4),$$

where R_{ct}^0 and R_{ct} and i_{corr}^0 and i_{corr} are the charge transfer resistances and corrosion current densities, respectively, with and without inhibitor, respectively.

The potential of zero charge (PZC) was calculated from the impedance measured at 298 K at various potentials in a corrosive solution containing 1.0 g/L WSLCE.

2.5 Surface analysis

After the samples were removed from the corrosive solution, their surfaces were thoroughly washed using distilled water and dried. Sample morphologies were then analyzed by scanning electronic microscopy (SEM) using TEDCAN VEGA 3 SBH instrument and by atomic force microscopy (AFM) using Bruker MULTIMODE 8 instrument. AFM was conducted using a tapping mode and a 2.5 Hz scan rate. ATR-FTIR analysis of the steel surface was performed using a Nicolet 10 instrument in the $600\text{-}4000 \text{ cm}^{-1}$ range. XPS spectra were recorded by the PHI5000-VersaProbe system using Mg K α radiation used as the excitation source.

3. RESULTS AND DISCUSSION

3.1 FTIR

FTIR spectrum of WSLCE showed a broad, but strong peak at 3398 cm^{-1} (Figure 1) attributed to the O-H bond stretching. Peaks at 2926 and 2866 cm^{-1} were attributed to the C-H vibrations. Strong peaks at 1647 and 1421 cm^{-1} were ascribed to the C=O stretching vibrations and the H-C-H bending, respectively. The absorption bands at 1514 and 1240 cm^{-1} were attributed to aromatic ring framework vibration. The strong peak at 1076 cm^{-1} very likely corresponded to the C-O-C stretching vibrations. Small peaks in the $1000\text{-}500\text{ cm}^{-1}$ range typically correspond to aromatic and aliphatic C-H groups. The presence of all these groups confirms that WSLCE was successfully obtained.

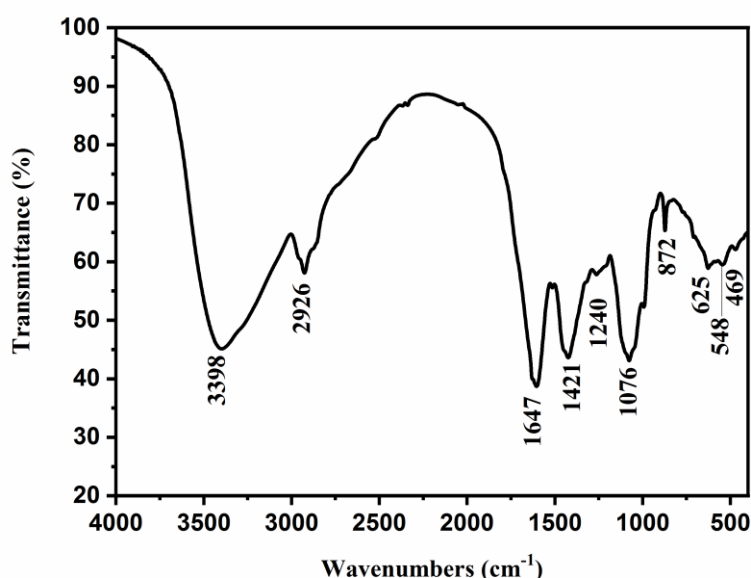


Figure 1. FTIR spectrum of WSLCE.

3.2 Gravimetric analysis

WSLCE inhibition efficiency (η) was excellent over a wide concentration range (from 0.1 to 1.0 g/L, see Table 1). η increased as WSLCE concentration in the corrosion solution increased and decreased as temperature during corrosion experiments was increased.

Table 1. Corrosion data obtained for the mild steel sample exposed to 1 M HCl solution containing 0-1.0 g/L WSLCE at 298, 308, and 318 K.

C (g·L ⁻¹)	298K			308K			318K		
	Δw (mg)	CR (mmpy)	η (%)	Δw (mg)	CR (mmpy)	η (%)	Δw (mg)	CR (mmpy)	η (%)
0	62.4	10.1	--	69.8	11.4	--	77.6	12.7	--
0.1	14.7	2.4	76.4	21.2	3.5	69.6	29.4	4.8	62.1
0.2	10.9	1.8	82.5	15.9	2.6	77.2	24.8	4.1	68.0
0.5	6.5	1.1	89.6	9.1	1.5	86.9	16.9	2.8	78.2
1.0	5.3	0.9	91.5	6.9	1.1	90.1	14.1	2.3	81.8

3.3 Impedance measurements

The Nyquist plots obtained for our steel samples at the open-circuit potential and immersed for 30 min in 1 M HCl (containing different contents of WSLCE) showed depressed capacitive semicircles, which we attributed to the 1) charge transfer reaction and time constant of the electric double layer and to 2) the surface or interfacial inhomogeneity similar to the one found in adsorption processes (Figure 2) [22, 23]. The Nyquist plots obtained for the samples treated at different corrosion conditions showed very similar shapes. Thus, the corrosion mechanisms of all these processes were the same. Semicircle diameters increased as the WSLCE content in the corrosion solution increased. This is strong evidence that the presence of WSLCE inhibited corrosion of our samples in HCl [24-26].

EIS data fitting was performed using an equivalent circuit shown in Figure 3.

R_s and R_{ct} are the solution, and the charge transfer resistances; CPE is the constant phase element. CPE impedance can be expressed, as shown below:

$$Z_{CPE} = \frac{1}{Y_0 (j\omega)^n} \quad (5),$$

where Y_0 is the CPE constant, n is a factor reflecting surface roughness, $j^2 = -1$ is an imaginary number, and ω is the angular frequency (in rad/s). At $n = 0, 1, 0.5$ and -1 CPE contribution is considered equal to a resistance ($Z_{CPE} = R$), capacitance ($Z_{CPE} = C$), Warburg impedance ($Z_{CPE} = W$) or an inductance ($Z_{CPE} = L$), respectively [27]. All these values calculated for our mild steel samples corroded in 1 M HCl at different temperatures and under the presence of different SWCLE contents (C) are listed in Table 2.

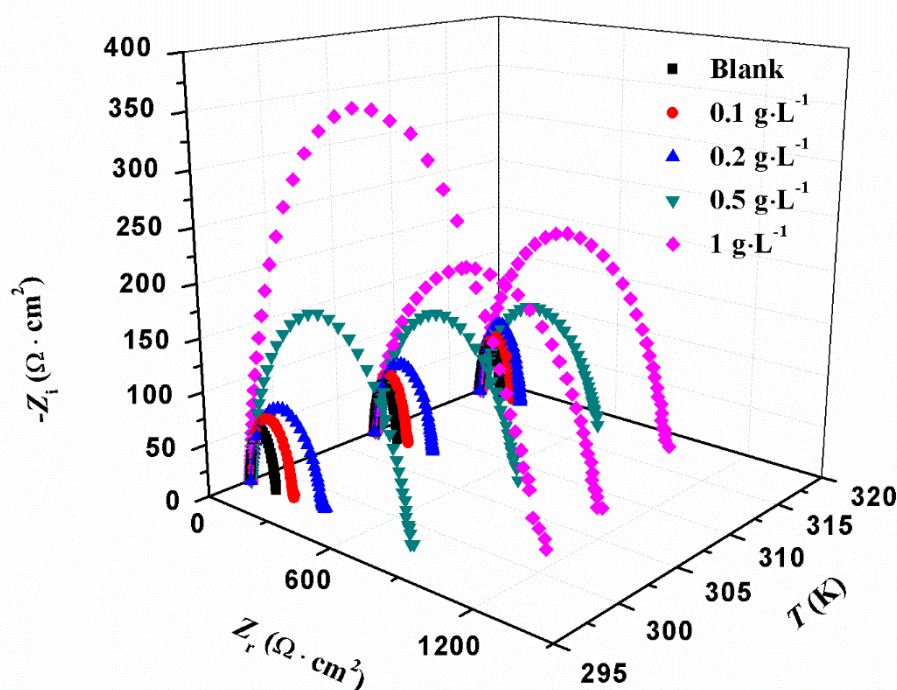


Figure 2. Nyquist plots for mild steel corroded in 1 M HCl containing 0-1.0 g/L WSLCE and at 298, 308, and 318 K.

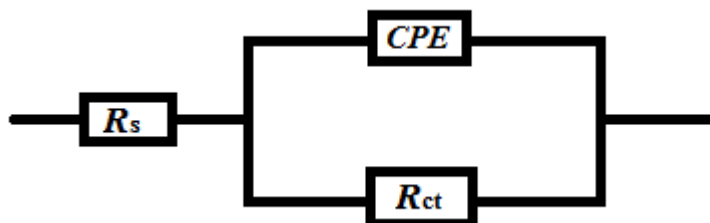


Figure 3. Equivalent circuit used to fit EIS data.

The R_{ct} values increased as WSLCE content in the corrosive solution increased while Y_0 values decreased. Thus, the amount of adsorbed WSLCE increased as it removed corrosive molecules (water and HCl) from the steel surface, decreasing their activity as well as the number of active sites participating in dissolution reactions. The maximum η_R values at 298 K, 308 K, and 318 K were equal to 89.6%, 88.4%, and 87.8%, respectively.

Table 2. EIS parameters for the mild steel samples corroded in 1 M HCl at different temperatures under the presence of different WSLCE concentrations

T (K)	C (g·L ⁻¹)	R_s (Ω·cm ²)	CPE		R_{ct} (Ω·cm ²)	η_R (%)
			Y_0 (μF·cm ⁻²)	n		
298	0	2.7	272.8	0.9	136.1	--
	0.1	2.9	255.3	0.8	229.4	40.7
	0.2	1.9	245.1	0.8	383.5	64.5
	0.5	2.7	176.1	0.8	786.3	82.7
	1.0	3.3	92.0	0.9	1304	89.6
308	0	2.1	252.7	0.9	123.8	--
	0.1	4.2	236.8	0.8	180.3	31.3
	0.2	3.0	226.8	0.8	301.6	59.0
	0.5	1.2	218.0	0.8	708.5	82.5
	1.0	2.7	182.8	0.8	1063	88.4
318	0	2.7	248.8	0.9	112.1	--
	0.1	3.2	224.9	0.9	174.3	35.7
	0.2	3.2	196.3	0.8	216.6	48.3
	0.5	2.7	169.5	0.8	598.7	81.3
	1.0	2.4	142.2	0.8	920.9	87.8

3.4 Polarization curves

The presence of inhibitors affects a cathodic component of the corrosion current density more than the anodic one because the cathodic evolution of H₂ is more suppressed than the anodic iron dissolution. Polarization curves reflecting anodic reactions occurring under the WSLCE presence overlapped and intersected the anodic curve for the blank solution at ~ -0.3 V because WSLCE very likely was desorbed from the steel surface at higher potentials. At -0.3 V, WSLCE was desorbed entirely

from the steel surface [28]. E_{corr} values under the WSLCE presence were very close to E_{corr} for the control (without WSLCE) experiments (Table 3). Therefore, the corrosion inhibition of steel in 1 M HCl by WSLCE belonged to a mixed type [23, 29, 30].

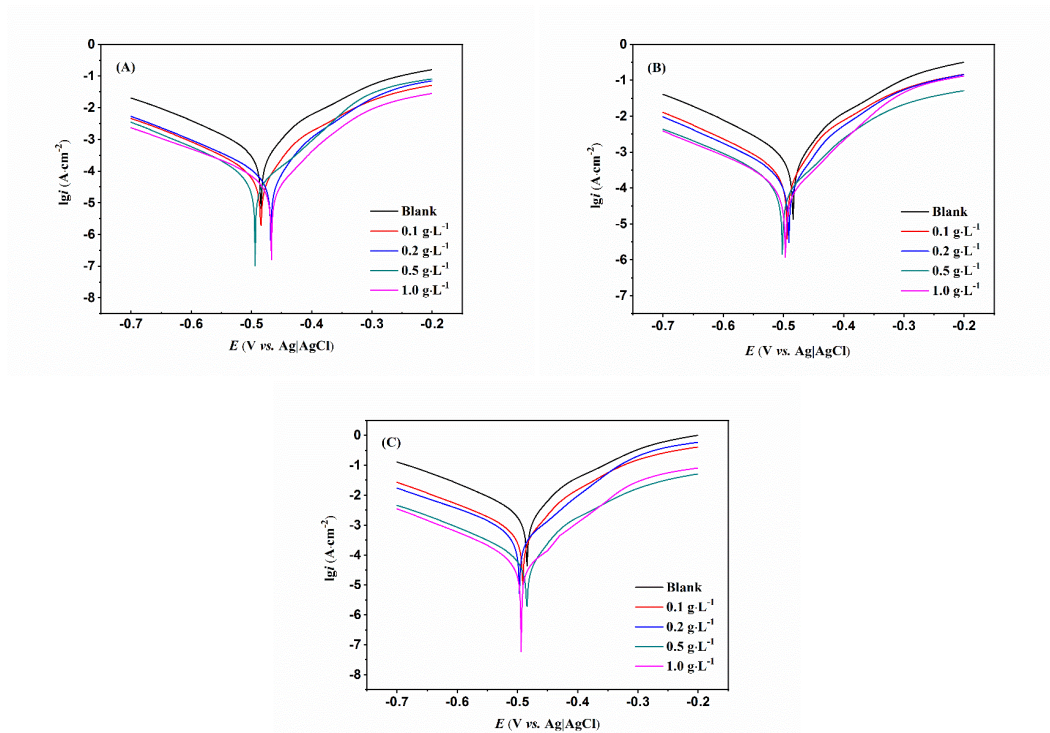


Figure 4. Polarization curves for the mild steel corroded in 1 M HCl containing 0-1.0 g/L WSLCE at (A) 298 K, (B) 308 K, and (C) 318 K.

Table 3. Polarization curve parameters of mild steel corroded in 1 M HCl containing different concentrations of WSLCE at different temperatures.

T (K)	C (g·L ⁻¹)	E_{corr} (mV)	i_{corr} ($\mu\text{A}\cdot\text{cm}^{-2}$)	η_i (%)
298	0	-484	331.1	--
	0.1	-485	29.4	91.1
	0.2	-468	26.7	92.0
	0.5	-492	24.5	92.6
	1.0	-468	21.6	93.5
308	0	-486	515.2	--
	0.1	-494	183.7	64.3
	0.2	-491	139.6	72.9
	0.5	-502	58.9	89.3
	1.0	-497	48.0	90.7
318	0	-487	1202	--
	0.1	-486	393.6	67.2
	0.2	-490	237.7	80.2
	0.5	-484	140.1	88.3
	1.0	-493	131.1	89.1

i_{corr} value, calculated using the Tafel extrapolation method, decreased after WSLCE was added (Table 3), which confirmed suppression of the corrosion reaction by the WSLCE film formed on the steel surface, which acted as a barrier between the metal and HCl.

Inhibition efficiency η increased as WSLCE concentration increased. At 1.0 g·L⁻¹ of WSLCE, η at 298, 308, and 318 K was equal to 93.5%, 90.7%, and 89.1%, respectively. These results agreed with the EIS data.

The anticorrosion performance of WSLCE was also compared with that of other extracts reported previously. The results are presented in Table 4, revealing that WSLCE shows a comparable or even better anticorrosion performance than the previously reported extracts.

Table 4. Comparison of the anticorrosion performance of WSLCE and other extracts

Extracts	Electrolyte solution	Optimum concentration	Temperature	Inhibition efficiency	Reference
Gum Arabic	1 M HCl	1.0 g/L	303K	97.0%	[31]
Brassica Campestris Extract	0.5 M H ₂ SO ₄	120ppm	293K	38.0%	[32]
Sargassum Muticum Extract	1 M HCl	1.5 g/L	303K	97.7%	[33]
Chicken Nails Extract	2 M H ₂ SO ₄	0.1 g/L	328K	74.0%	[34]
Castor Oil	1 M HCl	140 μmol/L	293K	82.0%	[35]
Hymenaea Stigonocarpa Extract	0.5 M H ₂ SO ₄	1233.4 mg/L	298K	87.2%	[36]
Lilium Brownii Leaves Extract	1 M HCl	200 mg/L	298K	84.3%	[37]
Stylosanthes Gracilis extract	1 M H ₂ SO ₄	1.2 g/L	298K	94.2%	[38]
Wintersweet Leaf Crude Extract	1 M HCl	1.0 g/L	298K	93.5%	This work

3.5 Adsorption tests

Organics adsorbed on the metal surface replaces initially present surface water molecules. Adsorption of WSLCE by the steel surface could be described by the Langmuir isotherm: [39]

$$\frac{\theta}{1-\theta} = K_{\text{ads}} C \quad (6),$$

where C is the WSLCE concentration, θ is the fraction of the surface coverage (obtained from weight loss data), and K_{ads} is the adsorption constant.

$\log(\theta/1-\theta)$ plotted as a function of $\log C$ showed linear dependency (see Figure 5), which confirms that WSLCE adsorption by the metal surface obeyed the Langmuir law.

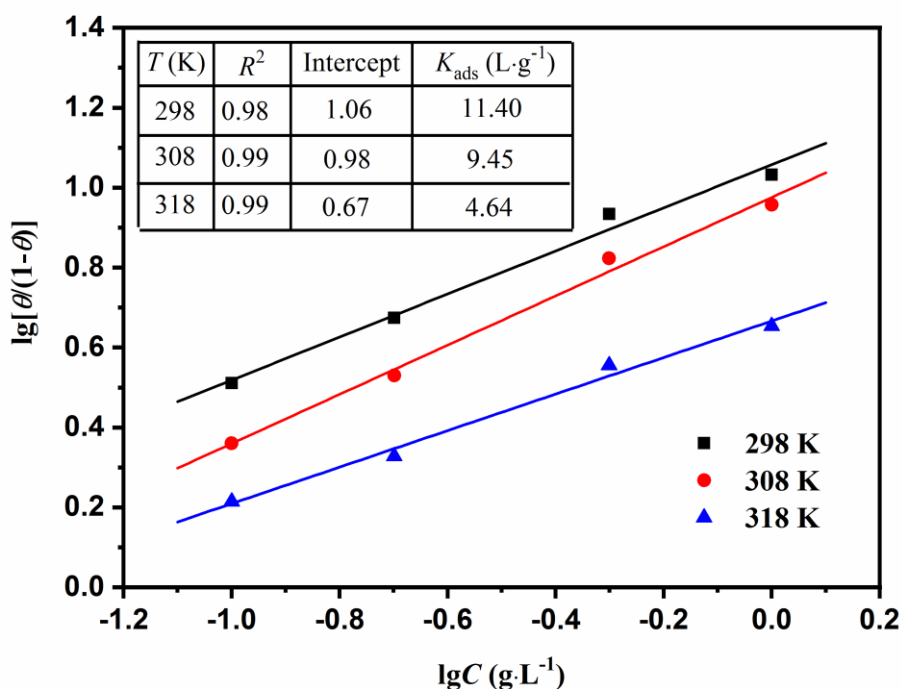


Figure 5. WSLCE adsorption isotherms by the mild steel conducted in 1 M HCl at 298 K, 308 K, and 318 K.

The high K_{ads} value reflects the high WSLCE adsorption capacity of the steel surface [40]. K_{ads} decreased as corrosion experiment temperature was increased. Thus, elevated temperatures hampered WSLCE adsorption.

The Gibbs free energy (ΔG^0_{ads}) of WSLCE adsorption by the steel surface can be evaluated as follows: [41]

$$K_{ads} = \frac{1}{C_{H_2O}} \exp\left(\frac{-\Delta G^0_{ads}}{RT}\right) \tag{7}$$

$\Delta G^0_{ads} > -20 \text{ kJ}\cdot\text{mol}^{-1}$ corresponds to physisorption, while $\Delta G^0_{ads} < -40 \text{ kJ}\cdot\text{mol}^{-1}$ corresponds to chemisorption.[42] ΔG^0_{ads} values for the corrosion under the WSLCE presence were in the $-22\sim-24 \text{ kJ}\cdot\text{mol}^{-1}$ range. Thus, spontaneous and energetically favored adsorption of WSLCE by the mild steel surface was very likely a combination of both physical and chemical adsorption.

Activation energies for our corrosion reactions, obtained from the equation shown below, are listed in Table 6:

$$\ln\left(\frac{r_2}{r_1}\right) = \frac{E_a(T_2 - T_1)}{RT_2T_1} \tag{8}$$

where r_1 and r_2 are the corrosion rates at temperatures T_1 and T_2 , respectively.

E_a increased as WSLCE concentration increased. Thus, WSLCE adsorbed on the steel surface strongly. The presence of WSLCE on the steel surface blocked the charge transfer between the steel and the surrounding corrosive environment, which slowed down the reaction and increased E_a [33-46].

The enthalpy and entropy of adsorption can be calculated from the following equations [47]:

$$\Delta H = E_a - RT \quad (9),$$

$$\Delta G = \Delta H - T\Delta S \quad (10),$$

Positive ΔH values indicate an endothermic reaction; thus, mild steel dissolution in 1 M HCl was energetically unfavorable (see Table 5) [48]. The positive value of the entropy change (ΔS) indicates a higher disorder due to the simultaneous WSLCE adsorption and water desorption [49].

Table 5. Entropy, enthalpy and Gibbs free energy of mild steel corrosion experiments conducted at 298 K, 308 K and 318 K in 1 M HCl under the presence of 1.0 g/L WSLCE.

T (K)	ΔH (kJ·mol ⁻¹)	ΔS (J·mol ⁻¹ ·K ⁻¹)	ΔG^0_{ads} (kJ·mol ⁻¹)
298	32.3	185.9	-23.1
308	32.2	180.6	-23.4
318	32.1	171.1	-22.3

Table 6. Activation energy of the mild steel corrosion reaction conducted in 1 M HCl under the presence of 0-1.0 g/L WSLCE

C (g·L ⁻¹)	E_a (kJ·mol ⁻¹)
0	9.2
0.1	27.9
0.2	33.0
0.5	38.5
1.0	39.5

3.6 Analysis of the potential of zero charge (PZC)

To further understand the mechanism of mild steel inhibition by WSLCE, we measured E_{pzc} and E_{OPC} (see Figure 6). The surface charge of the mild steel can be estimated using the equation shown [50]:

$$E_r = E_{OPC} - E_{PZC} \quad (11),$$

where E_r is the Antropov's "rational" corrosion potential.

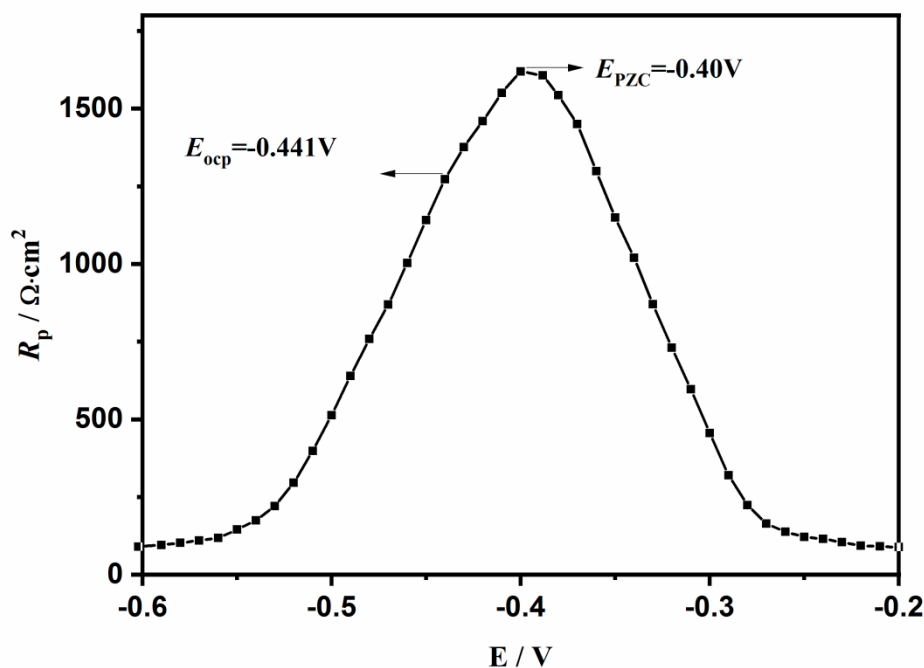


Figure 6. The plot of R_p vs. applied potential during mild steel corrosion in 1 M HCl under the presence of 1.0 g/L WSLCE.

The resulting data plot showed a parabolic shape with a maximum at -0.40 V (vs. Ag/AgCl, see Figure 6), which corresponded to the E_{PZC} obtained for the corrosion reaction under the presence of 1.0 g·L⁻¹ of WSLCE. E_{OCP} for the same conditions was more negative than the E_{PZC} : -0.441 V (vs. Ag/AgCl), which is indicative of the negatively charged surface after 30 min corrosion. The corresponding E_r value was equal to -0.041 V.

These results suggest that during the corrosion at these conditions, the active WSLCE form might be a protonated one. Protonated WSLCE molecules were very likely in equilibrium with the neutral HCl molecules. Such chemical configuration of WSLCE molecules was very favorable for their electrostatic interaction with the steel surface. At the same time, non-protonated WSLCE could be adsorbed on the metal surface by the donor-acceptor interactions between coupled electron pairs or π -electrons and empty d-orbitals of Fe [51]. Such an interaction would be considered chemical adsorption.

3.7 Surface analysis

SEM analysis of the mild steel surface corroded in 1 M HCl solution for 3 h showed severe surface deterioration, including visible damage, numerous pores, and a very uneven and thick corrosion layer (Figure 7a). However, when a steel surface was treated with WSLCE, only minimum surface degradation was observed (see Figure 7b): polishing markings could still be distinguished. Similar results were reported in the literature [52-54]. These results confirmed WSLCE ability to strongly adhere to the mild steel surface and to protect it from the corrosion.

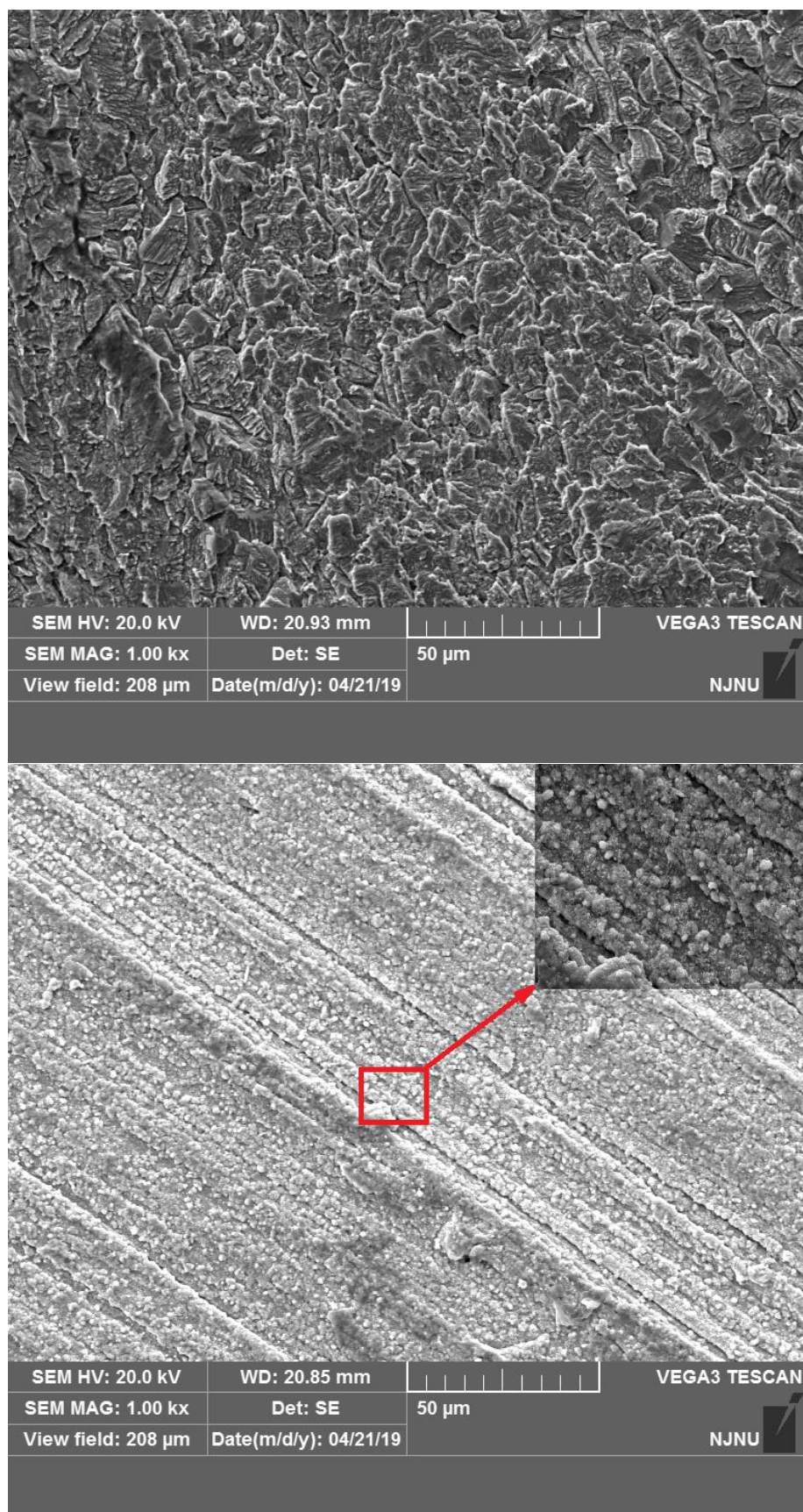


Figure 7. SEM micrographs of mild steel corroded in 1 M HCl without (a) and with (b) 1.0 g/L WSLCE.

AFM data collected for the steel corroded without WSLCE presence showed a very rough surface (with an average roughness features of ~19.7 nm). In comparison, the roughness of the steel corroded under the presence of 1.0 g/L was ~4.26 nm (Figure 8). These results support excellent inhibiting properties of WSLCE [54-56].

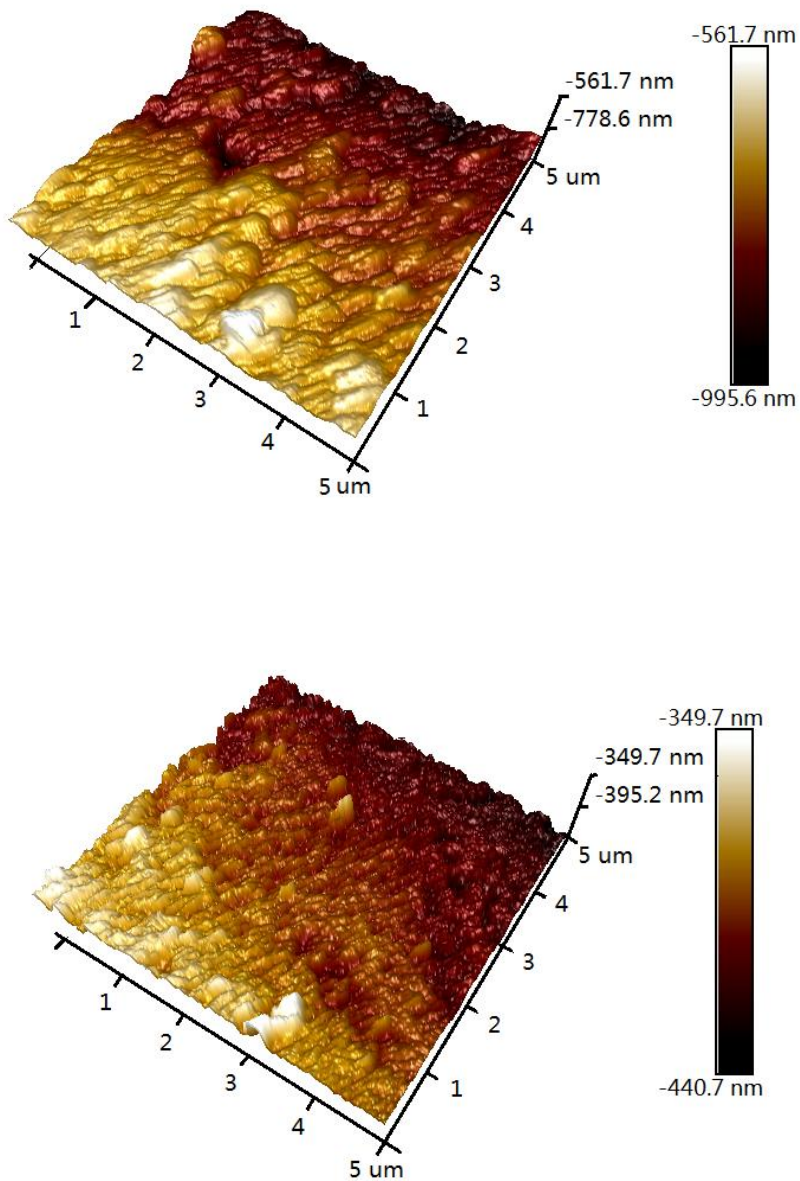


Figure 8. AFM of the mild steel corroded in 1 M HCl without (a) and with (b) 1.0 g/L WSLCE.

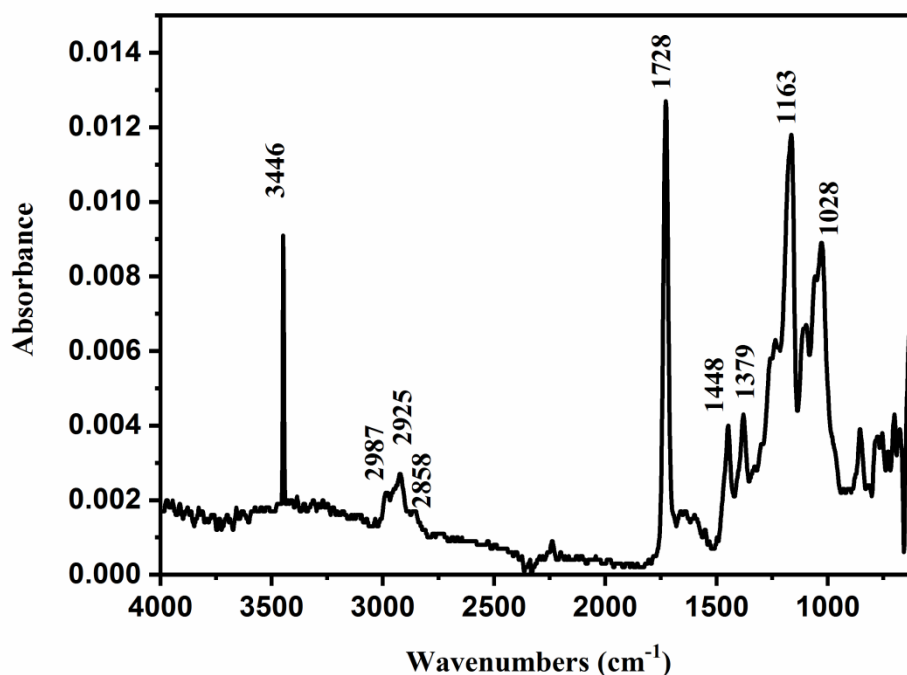
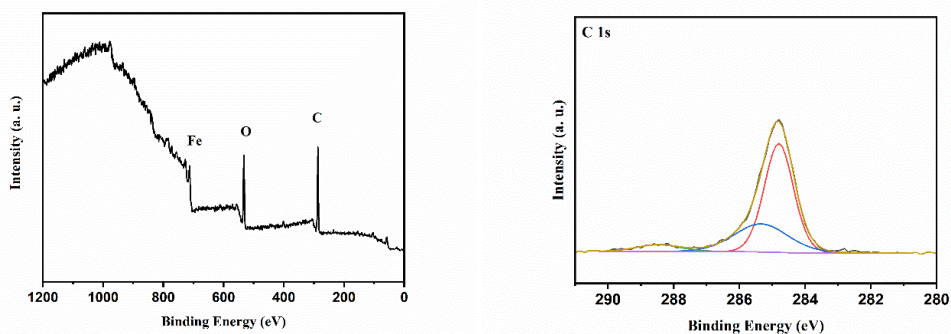


Figure 9. ATR-FTIR spectrum of WSLCE adsorbed on the mild steel surface.

ATR-FTIR spectra of the WSLCE adsorbed on the steel surface showed a band at 3430 cm^{-1} attributed to the O-H bond. FTIR peaks located at 2987 , 2925 , and 2858 cm^{-1} were attributed to aliphatic C-H stretching. Strong peaks at 1728 and 1448 cm^{-1} were assigned to C=O and C=C vibrations, respectively. Also, the C-H stretching vibrations of phenols or alcohols (typically positioned at 1379 , 1163 , and 1028 cm^{-1}) were visible. Series of smaller peaks in the $600\text{--}900\text{ cm}^{-1}$ region very likely corresponded to the Fe-O stretching vibration [57-60].

XPS of WSLCE layer adsorbed on the steel surface (corroded for 3 h in 1 M HCl containing 1.0 g/L of WSLCE) showed the presence of ferric oxide and organics judging by the appearance C 1s, O 1s, and Fe 2p peaks (see Figure 10 and Table 7).



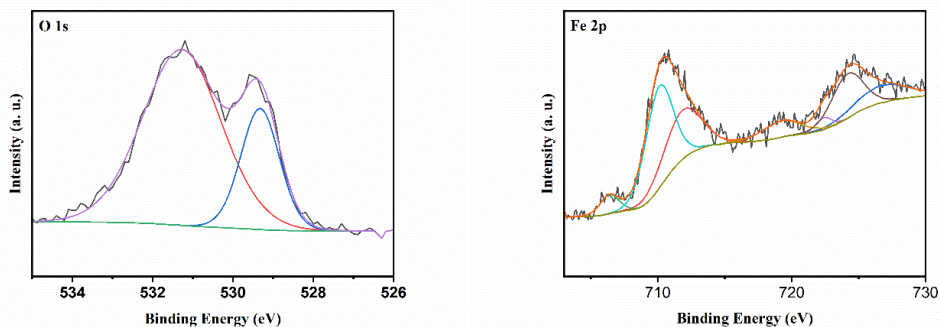


Figure 10. Full energy (a) and high-resolution C 1s (b), O 1s (c), and Fe 2p (d) XPS spectra of the mild steel sample after it corroded for 3 hours in 1 M HCl containing 1.0 g/L of WSLCE.

Table 7. XPS data of the mild steel corroded for 3 hours in 1 M HCl under the presence of 1.0 g/L WSLCE.

C		O		Fe	
BE (eV)	Bond	BE (eV)	Bond	BE (eV)	Bond
284.8(63.6%)	C-C	529.3(25.2%)	Fe ₂ O ₃	706.4(4.5%)	Fe ⁰
285.3(30.4%)	C-H	531.3(74.8%)	FeOOH	710.1(34.5%)	FeO
288.5(6.0%)	C-O			711.8(22.5%)	Fe ₂ O ₃ /Fe ₃ O ₄ /FeOOH
				719.3(7.9%)	Satellite of Fe (III)
				724.2(18.3%)	Fe 2p 1/2
				726.8(12.3%)	Fe 2p 1/2

C 1s peak was deconvoluted into three peaks. The most substantial peak (at 284.8 eV) was attributed to the aromatic bonds. Peaks at 285.3 and 288.5 eV corresponded to C-H and C-O bonds, respectively [61-63]. The O 1s spectrum was interpreted as a combination of two peaks: at 529.3 and 531.3 eV, which corresponded to O in oxides (Fe₂O₃ and/or Fe₃O₄) [64] and O in hydroxides (FeOOH and/or Fe(OH)₃) [64], respectively. The Fe 2p peak was deconvoluted into two peaks positioned at 711.8 and 724.2 eV, which correspond to Fe 2p_{3/2} and Fe 2p_{1/2}, respectively. Another peak located at 706.4 eV was attributed to the iron atom in the FeO configuration [65, 66]. The peak located at 711.8 eV corresponds to the ferric iron (e.g., FeOOH, Fe₂O₃, and/or Fe₃O₄) [67, 68]. A peak at 719.3 eV was ascribed to the Fe(III) satellite peak [65]. The presence of all these XPS peaks strongly supports WSLCE adsorption on the mild steel surface.

4. CONCLUSION

(1) Electrochemical analyses showed that the anticorrosion efficiency of WSLCE increased as its concentration in the corrosion solution was increased. However, with temperature, WSLCE inhibiting properties decreased. WSLCE acted as a mixed-type corrosion inhibitor.

(2) WSLCE adsorption on the mild steel followed the Langmuir adsorption law. The Gibb's free energy and PZC values indicate that both chemi- and physi-sorption took place.

(3) Adsorbed WSLCE acted as a protective film, efficiently preventing corrosion of the mild steel caused by the aggressive HCl medium.

ACKNOWLEDGEMENTS

The author gratefully acknowledges the support of Open Fund of Shandong Key Laboratory of Corrosion Science (KLCS201901), the Opening Project of Material Corrosion and Protection Key Laboratory of Sichuan province (2019CL14).

References

1. M. Allaoui, O. Rahim, L. Sekhri, *Orient. J. Chem.*, 33 (2017) 637.
2. H. Ashassi-Sorkhabi, D. Seifzadeh, M.G. Hosseini, *Corros. Sci.*, 50 (2008) 3363.
3. M. Elayyachy, A. El Idrissi, B. Hammouti, *Corros. Sci.*, 48 (2006) 2470.
4. K.C. Emregül, M. Hayvalı, *Corros. Sci.*, 48 (2006) 797.
5. M.A. Quraishi, D. Jamal, R.N. Singh, *J. Appl. Electrochem.*, 32 (2002) 425.
6. E.A. Noor, *Corros. Sci.*, 47 (2005) 33.
7. A. Popova, M. Christov, *Corros. Sci.*, 48 (2006) 3208.
8. J.D. Talati, D.K. Gandhi, *Corros. Sci.*, 23 (1983) 1315.
9. J. Halambek, K. Berković, J. Vorkapić-Furač, *Corros. Sci.*, 52 (2010) 3978.
10. P.C. Okafor, E.E. Ebenso, A.Y. El-Etre, M.A. Quraishi, *Int. J. Corros.*, 2012 (2012) 1.
11. A.M. Abdel-Gaber, B.A. Abd-El-Nabey, I.M. Sidahmed, A.M. El-Zayady, M. Saadawy, *Corros. Sci.*, 48 (2006) 2765.
12. E.E. Oguzie, *Corros. Sci.*, 50 (2008) 2993.
13. S. Mo, H.Q. Luo, N.B. Li, *Chem. Pap.* 70 (2016) 1131.
14. M. Bouklah, B. Hammouti, M. Benkaddour, T. Benhadda, *J. Appl. Electrochem.*, 35 (2005) 1095.
15. A.S. Fouda, A.A. Al-Sarawy, E.E. El-Katori, *Desalination*, 201 (2006) 1.
16. P.B. Raja, M.G. Sethuraman, *Mater. Lett.*, 62 (2008) 113.
17. B. Sanyal, *Prog. Org. Coat.*, 9 (1981) 165.
18. M. Abdullah Dar, *Ind. Lubr. Tribol.*, 63 (2011) 227.
19. A. Ait Aghzzaf, D. Veys-Renaux, E. Rocca, *Mater. Corros.*, 71 (2019) 148.
20. Y. Ueyama, S. Hashimoto, H. Nii, K. Furukawa, *Flavour Fragr. J.*, 5 (1990) 85.
21. M. Watanabe, J. Ayugase, *J. Sci. Food Agric.*, 95 (2014) 2095.
22. A. Pourghasemi Hanza, R. Naderi, E. Kowsari, M. Sayebani, *Corros. Sci.*, 107 (2016) 96.
23. Y. Qiang, S. Zhang, L. Guo, X. Zheng, B. Xiang, S. Chen. *Corros. Sci.*, 119 (2017) 68.
24. E. Gutiérrez, J.A. Rodríguez, J. Cruz-Borbolla, J.G. Alvarado-Rodríguez, P. Thangarasu, *Corros. Sci.*, 108 (2016) 23.
25. H. Tian, W. Li, B. Hou, *Corros. Sci.*, 53 (2011) 3435.
26. L. Hu, S. Zhang, W. Li, B. Hou, *Corros. Sci.*, 52 (2010) 2891.
27. B. Tan, S. Zhang, Y. Qiang, L. Feng, C. Liao, Y. Xu, S. Chen, *J. Mol. Liq.*, 248 (2017) 902.
28. Q. Wang, B. Tan, H. Bao, Y. Xie, Y. Mou, P. Li, D. Chen, Y. Shi, X. Li, W. Yang, *Bioelectrochemistry*, 128 (2019) 49.
29. Y. Yan, W. Li, L. Cai, B. Hou, *Electrochim. Acta*, 53 (2008) 5953.
30. B. Tan, S. Zhang, Y. Qiang, L. Guo, L. Feng, C. Liao, Y. Xu, S. Chen, *J. Colloid Interf. Sci.*, 526 (2018) 268.

31. K. Azzaoui, E. Mejdoubi, S. Jodeh, A. Lamhamdi, E. Rodriguez-Castellón, M. Algarra, A. Zarrouk, A. Errich, R. Salghi, H. Lgaz, *Corros. Sci.*, 129 (2017) 70.
32. M.P. Casaletto, V. Figò, A. Privitera, M. Bruno, A. Napolitano, S. Piacente, *Corros. Sci.*, 136 (2018) 91.
33. I. Nadi, Z. Belattmania, B. Sabour, A. Reani, A. Sahibed-dine, C. Jama, F. Bentiss, *Int. J. Biol. Macromol.*, 141 (2019) 137.
34. O. Olawale, J.O. Bello, B.T. Ogunsemi, U.C. Uchella, A.P. Oluyori, N.K. Oladejo, *Heliyon*, 5 (2019), e02821.
35. A. Farhadian, A. Rahimi, N. Safaei, A. Shaabani, M. Abdouss, A. Alavi, *Corros. Sci.*, 175 (2020) 108871.
36. E.B. Policarpi, A. Spinelli, *J. Taiwan Inst. Chem. E.*, 116 (2020) 215.
37. X.L. Zuo, W.P. Li, W. Luo, X. Zhang, Y.J. Qiang, J. Zhang, H. Li, B.C. Tan, *J. Mol. Liq.*, 321 (2021) 114914.
38. O.D. Ofuyekpone, O.G. Utu, B.O. Onyekpe, A.A. Adediran, *Sci. Afr.*, 11 (2021) e00714.
39. Y. Qiang, S. Zhang, S. Xu, L. Yin, *RSC Adv.*, 5 (2015) 63866.
40. G. Sığircık, T. Tüken, M. Erbil, *Corros. Sci.*, 102 (2016) 437.
41. N. El Hamdani, R. Fdil, M. Tourabi, C. Jama, F. Bentiss, *Appl. Surf. Sci.*, 357 (2015) 1294.
42. Z. Hu, Y. Meng, X. Ma, H. Zhu, J. Li, C. Li, D. Cao, *Corros. Sci.*, 112 (2016) 563.
43. S. Zor, P. Doğan, B. Yazıcı, *Corros. Rev.*, 23 (2005) 217.
44. M.M. Osman, R.A. El-Ghazawy, A.M. Al-Sabagh, *Mater. Chem. Phys.*, 80 (2003) 55.
45. D. Gopi, N. Bhuvaneshwaran, S. Rajeswarai, K. Ramadas, *Anti-Corros. Methods Mater.* 47 (2000) 332.
46. M.A. Ameer, E. Khamis, G. Al-Senani, *J. Appl. Electrochem.*, 32 (2002) 149.
47. L.M. Vračar, D.M. Dražić, *Corros. Sci.*, 44 (2002) 1669.
48. G.N. Mu, X. Li, F. Li, *Mater. Chem. Phys.*, 86 (2004) 59.
49. M.M. Saleh, *Mater. Chem. Phys.*, 98 (2006) 83.
50. A.O. Yüce, G. Kardaş, *Corros. Sci.*, 58 (2012) 86.
51. A. Kosari, M.H. Moayed, A. Davoodi, R. Parvizi, M. Momeni, H. Eshghi, H. Moradi, *Corros. Sci.*, 78 (2014) 138.
52. R. Yıldız, *Corros. Sci.*, 90 (2015) 544.
53. A. Rodríguez Torres, M.G. Valladares Cisneros, J.G. González Rodríguez, *Green Chem. Lett. Rev.*, 9 (2016) 143.
54. S. Varvara, R. Bostan, O. Bobis, L. Găină, F. Popa, V. Mena, R.M. Souto, *Appl. Surf. Sci.* 426 (2017) 1100.
55. C. Kamal, M.G. Sethuraman, *Mater. Corros.* 65 (2013) 846.
56. A. Dehghani, G. Bahlakeh, B. Ramezanzadeh, *Bioelectrochemistry*, 130 (2019) 107339.
57. T.A. Saleh, *J. Cleaner Prod.*, 172 (2018) 2123.
58. T.A. Saleh, S.O. Adio, M. Asif, H. Dafalla, *J. Cleaner Prod.*, 182 (2018) 960.
59. T.A. Saleh, M.M. Al-Shalalfeh, A.A. Al-Saadi, *Sci. Rep.*, 6 (2016) 32185.
60. T.A. Saleh, K.O. Sulaiman, S.A. Al-Hammadi, H. Dafalla, G.I. Danmaliki, *J. Cleaner Prod.* 154 (2017) 401.
61. J.F. Watts, J. Wolstenholme, *An Introduction to Surface Analysis by XPS and AES*, John Wiley and Sons Inc., (2003) London, UK.
62. C.D. Wanger, W.M. Riggs, L.E. Davis, J.F. Moulder G.E. Muilenberg, *Handbook of X-Ray Photoelectron Spectroscopy*, Perking-Elmer Corporation, Physical Electronics Divisionm, (1979) Minnesota, USA.
63. T. Yamashita, P. Hayes, *Appl. Surf. Sci.*, 254 (2008) 2441.
64. W. Temesghen, P. Sherwood, *Anal. Bioanal. Chem.*, 373 (2002) 601.
65. V. Di Castro, S. Ciampi, *Surf. Sci.*, 331 (1995) 294.
66. S.D. Zhang, J. Wu, W.B. Qi, J.Q. Wang, *Corros. Sci.*, 110 (2016) 57.

67. M.A. Pech-Canul, P. Bartolo-Pérez, *Surf. Coat. Tech.*, 184 (2004) 133.

68. F.Z. Bouanis, F. Bentiss, M. Traisnel, C. Jama, *Electrochim. Acta*, 54 (2009) 2371

© 2021 The Authors. Published by ESG (www.electrochemsci.org). This article is an open access article distributed under the terms and conditions of the Creative Commons Attribution license (<http://creativecommons.org/licenses/by/4.0/>).